Acta Biomaterialia 8 (2012) 2068–2076

Contents lists available at SciVerse ScienceDirect

Acta Biomaterialia

journal homepage: www.elsevier.com/locate/actabiomat

Charge binding of rhodamine derivative to OH^- stabilized nanomaghemite: Universal nanocarrier for construction of magnetofluorescent biosensors

Massimiliano Magro [a], Giulietta Sinigaglia [a], Luca Nodari [b], Jiri Tucek [c], Katerina Polakova [c], Zdenek Marusak [c], Sara Cardillo [a], Gabriella Salviulo [d], Umberto Russo [b], Roberto Stevanato [e], Radek Zboril [c,*], Fabio Vianello [a,*]

[a] Department of Biological Chemistry, University of Padua, Viale G. Colombo 3, 35121, Padua, Italy
[b] Department of Chemical Sciences, University of Padua, Via Marzolo 1, 35131 Padua, Italy
[c] Regional Centre of Advanced Technologies and Materials, Departments of Physical Chemistry and Experimental Physics, Faculty of Science, Palacky University in Olomouc, 17. Listopadu 1192/12, 771 46 Olomouc, Czech Republic
[d] Department of Geosciences, University of Padua, Viale Gradenigo 6, 35131 Padua, Italy
[e] Department of Physical Chemistry, Cà Foscari University in Venice, Dorsoduro 2137, 30123 Venice, Italy

ARTICLE INFO

Article history:
Received 11 October 2011
Received in revised form 3 February 2012
Accepted 6 February 2012
Available online 13 February 2012

Keywords:
Maghemite nanoparticles
Rhodamine isothiocyanate
Glucose oxidase nanocatalyst
Biosensor
OH^- groups

ABSTRACT

Superparamagnetic nanoparticles (20–40 nm) of maghemite, γ-Fe_2O_3, with well-defined stoichiometric structure, are synthesized by the borohydride reduction of ferric chloride at an elevated temperature (100 °C) followed by thermal treatment of the reaction product. Prepared maghemite nanoparticles reveal excellent colloidal stability for a long time without the necessity for any additional surface modification. These colloidal features are due to surface stabilizing OH^- groups, which act as charge barriers preventing a particle aggregation and enabling a reversible binding of various oppositely charged organic substances. Such binding with rhodamine B isothiocyanate results in the fluorescent magnetic nanocarrier providing, at the same time, a spacer arm for covalent immobilization of other biosubstances including enzymes. In this work, we exploit this general applicability of the developed nanocarrier for covalent immobilization of glucose oxidase. This is the first reported example of magnetically drivable fluorescent nanocatalyst. The immobilized enzyme creates a 3–5 nm thick layer on the nanoparticle surface as proved by high-resolution transmission electron microscopy. This layer corresponds to 10 enzyme molecules, which are bound to the nanoparticle surface as found by the fluorimetric determination of flavin adenine dinucleotide. The developed magnetic fluorescent nanocatalyst, showing a rate constant of 32.7 s^{-1} toward glucose oxidation, can be used as a biosensor in various biochemical, biotechnological, and food chemistry applications. The presence of the nanocatalyst can be simply monitored by its fluorescence; moreover, it can be easily separated from the solution by an external magnetic field and repeatedly used without a loss of catalytic efficiency.

1. Introduction

Magnetic nanoparticles of iron oxides, namely maghemite (i.e. γ-Fe_2O_3) and magnetite (i.e. Fe_3O_4), play a key role in modern biomedical and biotechnological applications. Among various magnetic species, nanosized iron-oxide-based magnetic particles possess many superior properties including magnetic (e.g. superparamagnetism, high values of saturation magnetization, easy control by small magnetic fields) and biochemical (e.g. non-toxicity, biodegradability, biocompatibility) characteristics [1–8] that empower their prominent application position in diverse fields of medicine.

Particles such as cross-linked iron oxide (CLIO) [9,10], ultrasmall superparamagnetic iron oxide (USPIO) [11–13], and monocrystalline iron oxide nanoparticles (MIONs) [14,15] have all been developed as imaging agents in magnetic resonance imaging (MRI). Some of the reported particles are likely to be taken up by macrophages and immune cells and can be used to image lymph nodes and inflammatory tissues.

Cell labeling is another biomedical field where iron oxide nanoparticles have been found very effective. Commonly, surfaces of magnetic nanoparticles are coated with compounds of mostly organic nature favoring either non-specific or specific cell labeling. Thus, a magnetic nanoparticle is functionalized with specific ligands for targeting cell membrane receptors. For example, Lunov

* Corresponding authors. Tel.: +420 585634947; fax: +420 585634761 (R. Zboril), tel.: +39 0498276863; fax: +39 0498073310 (F. Vianello).
E-mail addresses: zboril@prfnw.upol.cz (R. Zboril), fabio.vianello@unipd.it (F. Vianello).

1742-7061/$ - see front matter © 2012 Acta Materialia Inc. Published by Elsevier Ltd. All rights reserved.
doi:10.1016/j.actbio.2012.02.005

et al. [16] analyzed the effect of carboxydextran-coated superparamagnetic iron oxide (SPIO) and USPIO on c-Jun N-terminal kinase-mediated apoptosis in human macrophages. It has been demonstrated that after their uptake by macrophages, the nanoparticles induce a delayed apoptosis and their cytotoxicity significantly depends on the carboxydextran shell thickness. SPIO nanoparticles have been also shown to help track effectively the distribution and differentiation of progenitor and stem cells [17]. To achieve this, a cell labeling approach using short HIV-Tat peptides has been developed to derivatize SPIO nanoparticles, which are then internalized into hematopoietic and neural progenitor cells. To label human mesenchymal stem cells (hMSCs), fluorescein isothiocyanate (FITC)-incorporated silica-coated core–shell SPIO nanoparticles have been proved as suitable magnetic vectors exhibiting an intracellular localization in late endosomes/lysosomes [18]. If a removal of specific biological entities from their native environment is required, cell labeling is often followed by magnetic-field-based separation [19,20].

Magnetic nanoparticles have been also used as heating elements in tumor treatment employing magnetically induced hyperthermia procedures. It has been found that colloidal dispersions of SPIO (monodomain) nanoparticles exhibit an extraordinary specific absorption rate with the value much higher than that corresponding to the hysteresis heating of larger multidomain particles at clinically tolerable inductions and frequencies of alternating magnetic fields [21]. The effect of an external magnetic field on magnetic nanoparticles is also used in targeted drug delivery approaches. To achieve the highest efficiency of targeted drug delivery, size, charge, and surface chemistry of magnetic nanoparticles have to be considered. Surface modification of magnetic nanoparticles plays a very important role since it increases the time during which they are unrecognized by macrophages [1].

Magnetic particles have been also exploited to immobilize enzymes and other biosubstances in order to enhance their stability and enable their separation from the reaction mixture [22–26]. These magnetic immobilizations have been developed for applications in proteomics [27–30] or for construction of various biosensors [31–35]. Metal oxide nanoparticles can be functionalized with various biomolecules (e.g. redox enzyme) and may thus act as probes for biorecognition events. Glucose sensing applications of SPIO nanoparticles have been reported in the literature [36]; recently, an amperometric glucose biosensor based on an Fe_3O_4@SiO_2/carbon nanotube (CNT) architecture has been successfully employed in the detection of glucose [37]. It has been found that CNTs enhanced the electroactive surface area for a higher enzyme loading. In this context, a polyaniline coated CNT/Fe_3O_4 nanocomposite has been also proposed for glucose sensing [38]. The ability of CNTs to promote electron-transfer reactions in combination with high conducting properties of polyaniline remarkably improved the electrochemical sensitivity of as-developed glucose biosensors.

Combining suitably coated magnetic nanoparticles with fluorescence-emitting compounds empowers the applicability of such complexes in biomedical fields due to their multifunctional properties. Fluorescence-based biosensors designed for glucose monitoring have been recently discussed in detail in the excellent review paper by Barone and Strano [39]. They can be used as dual-modality imaging probes taking advantages of both nuclear magnetic and optical fluorescence imaging [40–43]. If further functionalized with a drug, they perform both imaging and treatment functions [44–46]. Fluorescent magnetic nanocomposites can be also exploited in cell tracking, cytometry, and magnetic separation. There are several kinds of fluorescent magnetic nanocomposites differing in the type of the fluorescent compound and the way it is bounded to the surface of a magnetic nanoparticle. In most cases, quantum dots of a semiconductor nature (e.g. CdSe, CdTe, CdS, ZnSe, etc.) are used as fluorescence emitting agents. Apart from semiconductor quantum dots, a significant fluorescence feature is exhibited by silica-based inorganic compounds. Concerning fluorescence capability, rhodamine, and its derivates, is a well known fluorophore, showing large extinction coefficients, high fluorescence quantum yields, and a remarkable photostability [47]. Thus, rhodamine derivates are currently widely used as fluorescent probes in biomedical fields [48].

If a magnetic nanoparticle is coated with a suitable enzyme, the synthesized complex can also work as a biocatalyst. The immobilization of enzymes on magnetic nanoparticles confers convenience in handling by using an external magnet, ease of separation from the reaction mixture and reuse, resulting thus in a low production cost. Moreover, binding to a nanoparticle often leads to an increase in the thermal stability and activity of an enzyme. Thus, magnetically controllable enzymes are highly promising in various biotechnological applications including proteomics, biosensing, and targeted enzyme transport [27,49,50].

Sugar metabolism alteration such as diabetes is a serious disease affecting the human population worldwide. It has been estimated that ~24 million people are currently suffering from insulin imbalance. Therefore, research on biosensing devices targeting sugar content and exploiting nanomaterials is a particularly important biomedical topic in the context of glucose determination in blood [51]. There are several works reporting immobilization of glucose oxidase on the surfaces of magnetic nanoparticles, working thus as a glucose sensor [25,52] monitoring the glucose concentration in the solution via changes in the fluorescence of the dye present in the nanocomposite shell [53]. However, a biocatalyst system consisting of magnetic nanoparticle, glucose oxidase, and rhodamine derivate has not been developed yet.

To the best of our knowledge, no examples of direct binding of fluorophores and/or enzymes on a surface of iron oxide nanoparticle (without the primary organic functionalization of the surface) have been reported in the literature yet. Commonly, the immobilization of fluorophores or any biosubstances requires the primary surface functionalization through various organic linkers (e.g. polyethylene glycol (PEG), polyvinyl acetate (PVA), chitosan, dextran). In this work, we present a peculiar nanosystem, synthesized in a simple way, in which a positively charged fluorescent shell (fluorescent molecules of rhodamine B isothiocyanate) is directly bound to a negatively charged metal oxide surface (modified by OH^- groups). This magnetic fluorescent complex, exhibiting colloidal properties, can be considered as a universal device on which various biomolecules can be covalently bound via the isothiocyanate group. This is demonstrated by binding of glucose oxidase, developing thus an effective fluorescent magnetically drivable nanocatalyst which retains its activity. The absence of a coverage shell guarantees a strong magnetic response and good performances in solution upon an external magnet application.

2. Materials and methods

2.1. Chemicals

Chemicals were purchased at the highest commercially available purity and used without further treatment. Iron(III) chloride hexahydrate, sodium borohydride ($NaBH_4$), rhodamine B isothiocyanate (RITC), ammonia solution (25% in water), and HEPES (4-(2-hydroxyethyl)-1-piperazine-ethanesulfonic acid) were obtained from Aldrich (Sigma–Aldrich, Italy). Glucose oxidase (GOx) (EC 1.1.3.4), from Aspergillus niger, VII-S type, characterized by a specific activity of 285 U mg^{-1} protein, was purchased from Sigma (Gillingham, UK). Flavin adenine dinucleotide (FAD) was purchased from Fluka (Buchs, Switzerland). Milli-Q grade water was used. GOx purity was checked, for each enzyme lot, by acquiring UV–Vis spectra of

enzyme solutions. The highly purified GOx optical spectrum contains two maxima, i.e. at 450 and 280 nm, characterized by extinction coefficients of $2.82 \times 10^4\ M^{-1}\ cm^{-1}$ and $3.10 \times 10^5\ M^{-1}\ cm^{-1}$, respectively [54,55]. The absorbance values of solutions at known weight-to-volume concentration, acquired at 450 and 280 nm, were used to determine the enzyme purity, which was found to be higher than 95%.

2.2. Synthesis of bare maghemite nanoparticles – magnetic carrier (FeNp)

A typical synthetic procedure involves several steps. 10 g of $FeCl_3{\cdot}6H_2O$ was dissolved in 800 ml of MilliQ grade water under vigorous stirring at room temperature. 2 g of $NaBH_4$ solution in ammonia (3.5%, 100 ml) was then quickly added to the mixture. The system turned immediately to a black colour. In a short time after the reduction reaction occurrence, the temperature of the system was increased to 100 °C and kept constant for 2 h. It should be noted that if the procedure is carried out at room temperature, the resulting product is unstable in air and has a tendency to oxidize, giving a non-magnetic brown material within a few hours. On the contrary, the product prepared at an elevated temperature (100 °C) is characterized by a high stability and strong magnetic response. After 2 h of aging at room temperature, this magnetic product was separated by application of an external magnet and washed several times with water. In the final stage, the magnetic phase was thermally treated at 400 °C for 2 h. The final mass of product was 2.0 g of iron oxide and a yield of 68% was calculated. The obtained iron oxide nanoparticles (FeNp) were dispersed in 3.5 l of MilliQ grade water by treatment in an ultrasonic bath at 48 kHz, 50 W (Bransonic, model 221), for 3 h, which gave a colloidal suspension showing the colloidal stability for the monitored period (6 months).

2.3. Preparation of rhodamine B isothiocyanate bound maghemite nanoparticles – magnetic fluorescent carrier (FeNp-RITC)

Iron oxide nanoparticles can be superficially and reversibly modified by simple incubation in water in the presence of RITC, thus forming the magnetic fluorescent carrier. In a standard experiment, a suspension (50 ml) containing nanoparticles with a mass concentration of 200 mg l^{-1} binds 99.75 μmol of RITC per 1 g of FeNp, followed by the incubation in the presence of 300 μM RITC for 1 h at room temperature. The amount of the bound RITC was calculated from the disappearance of the absorbance at 554 nm in the supernatants (extinction coefficient $6.6 \times 10^4\ M^{-1}\ cm^{-1}$). Control experiments showed that RITC can be completely removed from the maghemite surface by incubation in concentrated (1 M) ammonium hydroxide. The released RITC matched the amount of rhodamine consumed from the initial incubated solution. Then, the FeNP-RITC composite was washed with water, and no leached rhodamine was detected in the washings by fluorescence spectroscopy. Previously, a calibration curve was established by determining RITC fluorescence at an excitation wavelength of 554 nm, emission wavelength of 580 nm, and a bandwidth of 2 nm, all being the acquisition parameters. The calibration curve was found to be linear in the 0.1 nM–1 μM RITC concentration range, and a detection limit of 0.1 nM was calculated.

2.4. Preparation of GOx-rhodamine-maghemite nanoparticles – magnetic fluorescent nanocatalyst (FeNp-RITC-GOx)

RITC can be used as a spacer arm due to the isothiocyanate groups to which primary amino groups of suitable organic molecules can be covalently linked. Exploiting this binding capability of RITC, GOx molecules were bound to the FeNp-RITC complex, thus resulting in the formation of a magnetically drivable fluorescent nanocatalyst of an FeNp-RITC-GOx architecture. The binding reaction was performed by adding 10 μM GOx in water to a solution containing FeNp-RITC complex and subsequent stirring overnight at 4 °C. The unbound enzyme was removed by an extensive nanoparticle washing employing an external magnetic field.

2.5. Determination of the amount of GOx bound to maghemite nanoparticles

The surface density of GOx molecules bound to FeNp-RITC nanoparticles was measured by a method exploiting the fluorimetric determination of FAD, i.e. the enzyme cofactor. This method is based on the release of the FAD molecules of GOx by incubation of the enzyme in acid solutions [56]. The released FAD molecules were measured by fluorescence spectroscopy. GOx immobilized on the FeNp-RITC complex was measured incubating the nanoparticle suspension in a test tube with 1 ml of 0.1 M HCl at pH = 1.0. The test tube was gently shaken end-over-end for 30 min at 4 °C and the solution containing the FAD molecules was treated with an external magnetic field to remove nanoparticles and used for the fluorimetric determination. A calibration curve was established with FAD and native GOx. The calibration curve of GOx was obtained by incubation of known amounts of the enzyme at 4 °C in 0.1 M HCl at pH = 1.0 for 30 min. FAD released was determined fluorometrically, exciting at 445 nm and reading at 550 nm. The calibration curve was found to be linear in the GOx concentration range of 10 nM–1 μM ($r > 0.99$); the sensitivity is 0.83 (±0.02) fAU nM^{-1}, which is 2.05 times higher than that obtained for the calibration curve of FAD. This result demonstrates that FAD is quantitatively removed from GOx [57]. The method is characterized by a GOx detection limit of 1.5 nM ($S/N = 3$).

2.6. Determination of enzyme activity

A spectrophotometric assay was used to measure the activity of free GOx in the solution as well as GOx immobilized on the nanoparticle surface. Initial kinetic measurements were carried out according to the peroxidase-coupled assay reported by Stevanato et al. [58]. H_2O_2 produced during the β-D-glucose oxidation was continuously monitored by a change in the absorbance at 555 nm, under continuous stirring, and using an extinction coefficient of $12500\ M^{-1}\ cm^{-1}$. Measurements were carried out in 20 mM HEPES (4-(2-hydroxyethyl)-1-piperazine-ethanesulfonic acid) at pH = 7.5.

2.7. Characterization of magnetic nanoparticles and magnetic fluorescent catalyst

Transmission electron microscopy (TEM) images were obtained using a JEM2010 microscope operated at 200 kV with a point-to-point resolution of 1.9 Å. Before measurements, the samples were dispersed in ethanol and the suspension was treated in ultrasounds for 10 min. A drop of very dilute suspension was placed on a carbon-coated grid and allowed to dry by evaporation at ambient temperature. Scanning electron microscopy (SEM) images were measured on a Hitachi SU-6600 microscope (FEG, SE image resolution of 1.2 nm at 30 kV). Zero-field Mössbauer spectra were recorded at 5 and 300 K in a constant acceleration mode with a 50 mCi $^{57}Co(Rh)$ source. The values of the isomer shift are reported with respect to α-Fe at room temperature. In-field Mössbauer measurements were performed in a constant acceleration mode when the sample was placed in a cryomagnetic system (Oxford Instruments) at a temperature of 5 K and exposed to an external magnetic field of 5 T, applied parallel to the direction of γ-rays. A superconducting quantum interference device (SQUID, MPMS XL-7 type, Quantum Design) was used for the magnetic

measurements. The hysteresis loops were collected at a temperature of 2 and 300 K in external magnetic fields ranging from −7 to +7 T. Simultaneous thermogravimetric (TG) analysis and differential scanning calorimetry (DSC) were performed by an STA 449 C Jupiter (Netzsch Instrument) coupled with a QMS 403 Aëolos mass spectrometer (Netzsch Instrument). The device supports TG/DSC measurements at temperatures ranging from room temperature to 1400 °C. TG and DSC resolution is 0.1 μg and 1 μW, respectively. The mass spectrometer operates in the range from 1 to 300 amu with a Faraday and SEV (Channeltron) detector. Optical spectroscopy and fluorescence measurements were performed by a Cary 50 spectrophotometer and by a Cary Eclipse fluorescence spectrometer (Varian Inc., Palo Alto, CA, USA), respectively, in quartz cuvettes (1 cm p.l.). Fourier transform infrared (FTIR) spectra were acquired using a Thermo Nicolet Nexus 670 instrument. Nanoparticle samples were homogenized with an anhydrous KBr powder and pelletized by a hydraulic press at 8 t. For dynamic light scattering and zeta-potential measurements of a nanoparticle suspension, a Zetasizer instrument (Malvern Instruments Ltd.) was employed.

3. Results and discussion

3.1. Synthesis and properties of colloidal maghemite/OH^- nanocarrier

Magnetic nanoparticles prepared by the developed wet chemical procedure, followed by a solid-state heating, exhibit a relatively uniform size distribution (20–40 nm) and well-defined globular shape as evidenced by microscopic (TEM and SEM) observations (see Fig. 1). Selected area electron diffraction (SAED) pattern is well ascribed to maghemite (i.e. γ-Fe_2O_3) and/or magnetite (i.e. Fe_3O_4) spinel structure (with two crystallographically non-equivalent cation sites – tetrahedral (T) and octahedral (O) sites), in a full accordance with XRD data (not shown).

Structural and magnetic properties of as-prepared iron oxide nanoparticles were investigated by zero-field and in-field Mössbauer spectroscopy, and SQUID magnetization measurements.

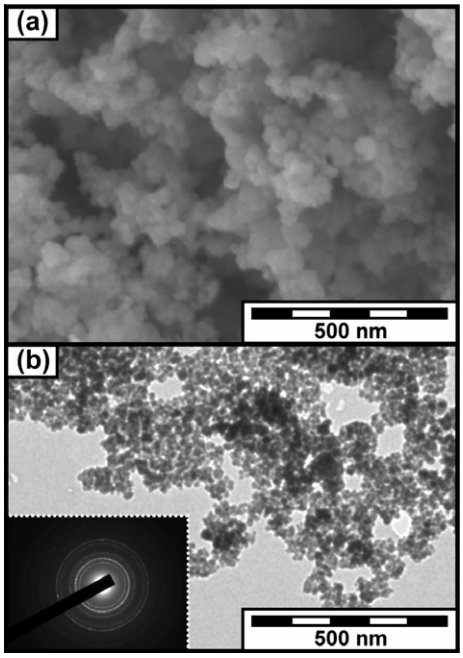

Fig. 1. (a) SEM and (b) TEM image of native magnetic nanoparticles demonstrating a quite uniform size distribution and globular shape of nanoparticles. SAED pattern, shown in the inset, corresponds well to the spinel structure of maghemite/magnetite.

In-field Mössbauer spectroscopy was used due to its unique ability to distinguish between structurally isomorphous maghemite and magnetite and also to quantify the distribution of cations in tetrahedral an octahedral sites of these spinel structures. The in-field Mössbauer spectrum collected at 5 K in an external magnetic field of 5 T, oriented in a parallel direction with respect to γ-ray propagation, is composed of two sextets, differing in the values of the hyperfine parameters (see Fig. 2 and Supplementary Table 1). These values of the hyperfine parameters correspond well with those reported for maghemite, when the Sextet 1 is ascribed to Fe^{3+} ions occupying the octahedral sites whereas the Sextet 2 arises from Fe^{3+} ions located at the tetrahedral sites of the maghemite spinel structure [59,60]. The ratio of the spectral area of the octahedral sextet to the spectral area of the tetrahedral sextet is equal to 5:3, which reflects the occupation of individual sites by Fe^{3+} ions. Taking into account the maghemite stoichiometric formula, given by $(Fe^{3+})^{T}(Fe^{3+}{}_{5/3}o_{1/3})^{O}O_4$, where o stands for vacancies, the prepared maghemite is perfectly stoichiometric. In this place, it is also worth mentioning that the alignment of ion magnetic moments within a nanoparticle can be monitored using in-field Mössbauer spectroscopy. In a parallel experimental geometry, if ion magnetic moments are completely aligned in the

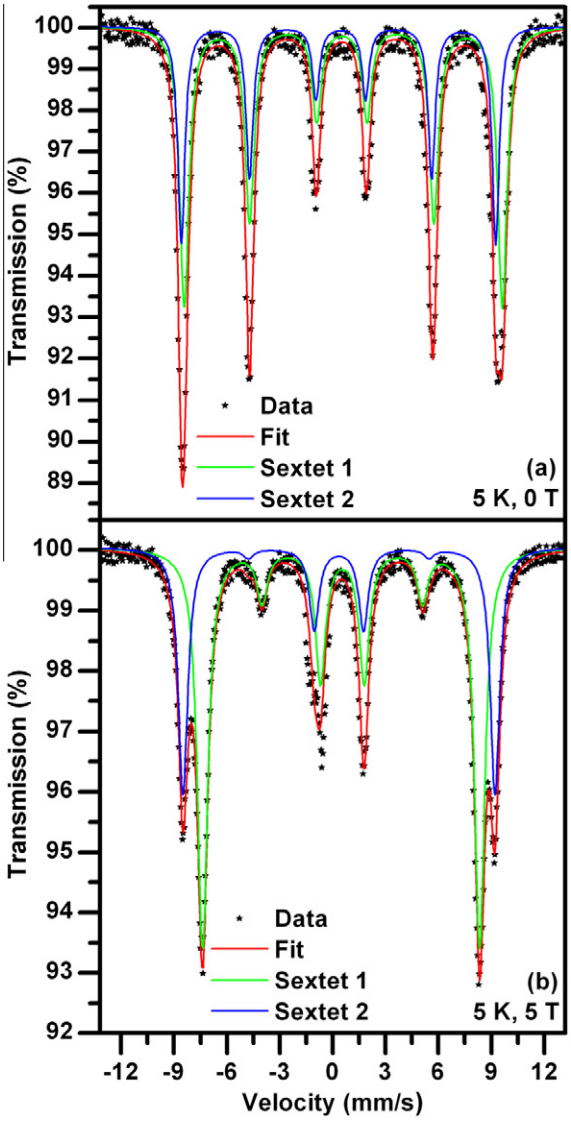

Fig. 2. (a) Zero-field and (b) in-field low-temperature Mössbauer spectrum of maghemite nanoparticles confirming their well defined and stoichiometric structure.

direction of an external magnetic field, zero intensity of the second and fifth spectral line in the in-field Mössbauer spectrum are expected. In our case, the observed non-zero intensity of the second and fifth spectral line (see Fig. 2) indicates some misalignment of atomic magnetic moments within the nanoparticle, implying the presence of a spin canting phenomenon, which is commonly observed in the nanopowdered systems [60].

To monitor the magnetic response of the nanopowder, hysteresis loops were measured at 2 and 300 K (see Fig. 3 and Supplementary Table 2). At 2 K, the isothermal magnetization curve shows hysteresis with the values of coercivity and remanent magnetization comparable with those reported for bulk maghemite (see Supplementary Table 2). The value of the maximum magnetization at 7 T is slightly lower than that reported for bulk maghemite, which is caused by a nanometer size of the particles. The hysteresis loop at 2 K is symmetric (i.e. equal values of the positive and negative coercivity, and positive and negative remanent magnetization) and no exchange bias phenomenon is present. Thus, the degree of magnetic disorder occuring at the surface layers of nanoparticles is not significant. Some misalignment of the surface atomic magnetic moments of each particle is present, in accordance with in-field Mössbauer data; however, it does not crucially govern the overall magnetic response of the system. At 300 K, the hysteresis is still observed and is a manifestation of the blocked state of the largest particles in the assembly. From the application viewpoint, it is important that a very high magnetization is achievable already at very low applied fields at room temperature.

Thus, we can conclude that the prepared magnetic particles would act as an excellent magnetic carrier due to their well defined stoichiometric structure, single-phase character, suitable magnetic properties, and quite uniform size distribution. Moreover, as a unique aspect of the preparation procedure, the particles exhibit colloidal behaviour with no indications of the sedimentation and/or aggregation process even within several days (see Fig. 4).

These visually observable excellent colloidal properties motivated us to perform a deeper analysis of the surface characteristics of the prepared maghemite nanoparticles and mechanism of their formation. Assuming the expected primary formation of nanoscale zero-valent iron (nZVI) as also proved by Mössbauer spectroscopy (not shown), we believe that the colloidal behaviour of nZVI particles with evidently suppressed interparticle interactions is related to the surface stabilization of maghemite by OH^- groups formed as summarized by the reaction equation given as

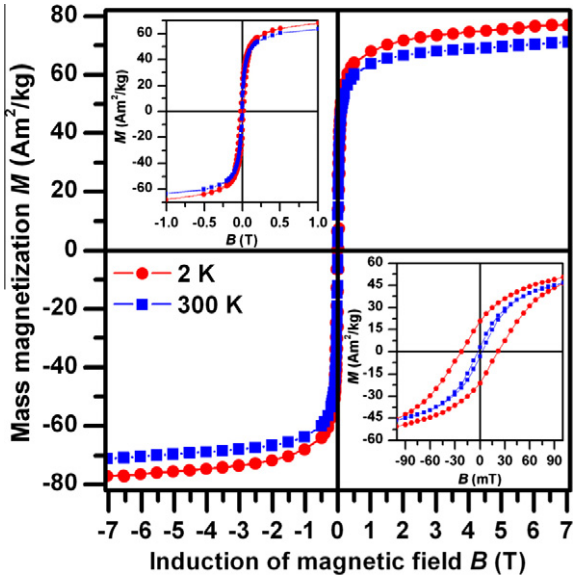

Fig. 3. Low- and room-temperature hysteresis loop of maghemite nanoparticles.

Fig. 4. Photographs of maghemite nanoparticles, stored three days in water, as demonstration of their excellent colloidal behaviour: water dispersions with maghemite nanoparticle concentrations of (a) 3.2 mg l^{-1} and (b) 0.1 mg l^{-1}.

$$Fe + 2H_2O + 1/2O_2 \rightarrow Fe^{3+} + 3OH^- + 1/2H_2 \quad (1)$$

The OH^- groups on the maghemite surface may act as a charge barrier preventing the particle aggregation and magnetic interactions of particles in dispersion. This is further supported by evolved gas analysis, where a release of OH^- groups was detected at temperatures higher than 300 °C (see Fig. 5a) (where a H_2O molecule release was detected, possibly coming from 2 vicinal OH^- groups substituted on the nanoparticle surface by an oxygen atom). Furthermore, the FTIR spectrum of freshly prepared nanoparticles, suspended as colloidal suspension by an ultrasonic bath, dried by lyophilization, and kept in an oven at 110 °C overnight before measurements (obtained by the solution method and consequent thermal treatment at 400 °C for 2 h) (see Fig. 5b), confirms the presence of OH^- groups witnessed by a peak centered at 869 cm^{-1}, which is clearly attributable to Fe–OH stretching mode [61]. The infrared spectrum, acquired in the region of 400–800 cm^{-1}, showed characteristic features of maghemite (absorptions present at 445 and 630 cm^{-1}), indicating cation vacancies [62,63].

Maghemite nanoparticles can be suspended in 0.05 M tetramethylammonium perchlorate by treatment in an ultrasonic bath at 48 kHz, 50 W, providing a stable colloidal suspension. The kinetics of the re-suspension phenomenon follows an exponential rise (see Supporting information, Fig. S1) and it was studied as a function of pH. The first-order kinetic constant of the re-suspension increases with increasing pH (from 1.0 h^{-1} at pH = 4.0 to 4.8 h^{-1} at pH = 11.0), confirming the involvement of solution OH^- groups in the colloidal suspension properties of nanoparticles (see Supporting information, Fig. S1). Moreover, in order to get more information on the properties of colloidal suspensions of maghemite nanoparticles, dynamic light scattering analysis and zeta potential measurements were performed in 0.05 M tetramethylammonium

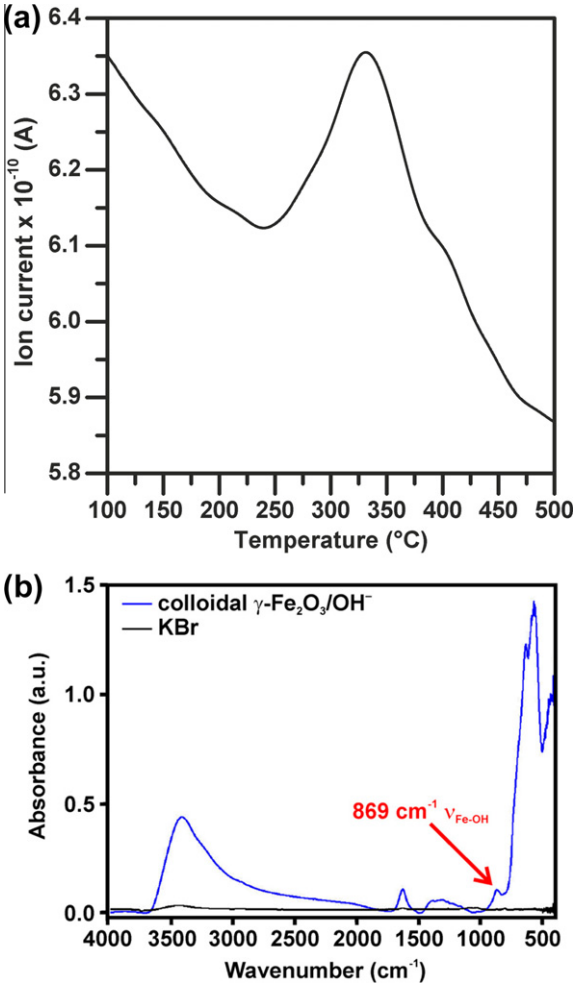

Fig. 5. (a) Evolved gas analysis indicating the evolution of H_2O molecules (OH^- groups) at ~330 °C and (b) FTIR spectrum confirming the presence of Fe–OH stretching vibrations.

perchlorate (pH = 7.0). Under these conditions, the hydrodynamic diameter of maghemite nanoparticles was found to be 50 nm and a zeta potential of –22.5 mV was determined. Generally, the hydrodynamic diameter is in good correspondence with TEM data, which, however, bring a more objective information on the real particles size. Zeta potential value gives an unambiguous evidence for the negative surface charge of nanoparticles, in accordance with FTIR and evolved gas analyses.

3.2. Surface coating of maghemite/OH^- nanoparticles (FeNp) with rhodamine B isothiocyanate (RITC) as a fluorescent label

Maghemite nanoparticles, as a colloidal suspension, can be superficially and reversibly labeled by a simple incubation in water in the presence of RITC. The amount of the bound fluorescent probe is dependent on the concentration of nanoparticles and RITC. In a standard experiment, a suspension (50 ml) containing nanoparticles with a mass concentration of 200 mg l^{-1} binds 99.75 μmol of RITC per 1 g of FeNp, followed by the incubation in the presence of 300 μM RITC for 1 h at room temperature. In order to determine the amount of RITC bound to the maghemite nanoparticles, the optical spectrum of the fluorescent probe in the solution was monitored during the binding procedure. To do so, we chose a wavelength of 554 nm corresponding to the position of the absorption maximum characterized by a molar extinction coefficient of 6.6×10^4 M^{-1} cm^{-1}. The amount of bound RITC was then calculated from the disappearance of the absorbance at 554 nm in the supernatants.

To confirm the expected electrostatic interaction mechanism of RITC with the maghemite/OH^- carrier, fluorescein isothiocyanate (FITC) was also tested as a structurally similar fluorescent probe. Differences in the chemical structures of RITC and FITC include, among others, the presence of positively charged nitrogen groups in the rhodamine molecules, which are substituted by hydroxyls in the fluorescein structure (see Supporting information, Fig. S2). As a result, the fluorescein derivative does bind to a nanoparticle surface, confirming the involvement of negative hydroxyls groups on the nanoparticle surface, giving thus a negative surface charge which is able to establish electrostatic interactions with the positively charged portion of rhodamine derivative.

TEM micrographs show the efficient coating of negatively charged maghemite/OH^- nanoparticles with a positively charged rhodamine shell, thus creating the magnetic fluorescent carrier. The average shell thickness, as estimated from high resolution TEM images, ranges between 2 and 4 nm (see Fig. 6 and compare with Fig. S3 given in the Supporting information).

The fluorescence characteristics of maghemite/OH^-/RITC were determined in comparison with free rhodamine. Upon immobilization, the quantum yield of the immobilized RITC decreased to 8.6 ± 1.6% of the rhodamine quantum yield, which is sufficient to apply the developed material as a magnetic fluorescent probe.

3.3. Glucose oxidase bound to rhodamine modified maghemite nanoparticles – properties of magnetic fluorescent nanocatalyst (FeNp-RITC-GOx)

GOx is one of the most used oxide-reductase in the enzyme-based biosensors since it catalyzes the oxidation of β-D-glucose to D-glucolactone with the production of hydrogen peroxide [64].

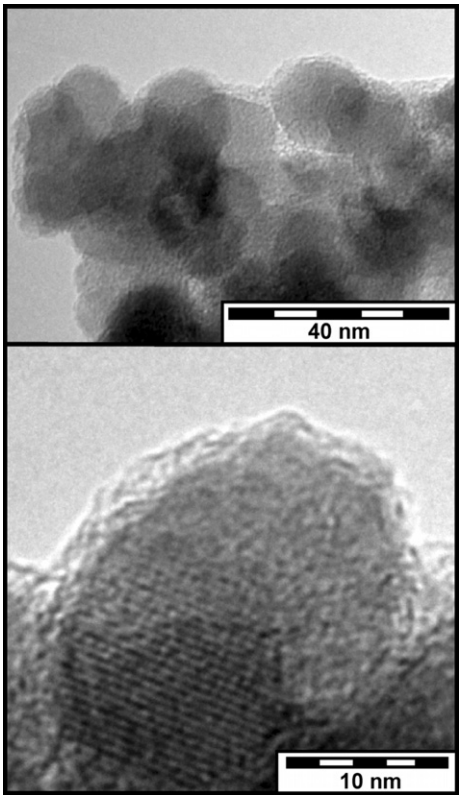

Fig. 6. TEM images of maghemite/OH^-/RITC nanoparticles demonstrating the rhodamine shell on the maghemite surface.

With the aim of developing the first GOx-based magnetic fluorescent biosensor, we immobilized GOx on the surface of rhodamine modified maghemite nanoparticles. RITC can be used as a spacer-arm, presenting the isothiocyanate functionality, to which primary amino groups of selected molecule can be covalently bound, thus forming magnetically drivable fluorescent biosensors. In the present work, the binding reaction was achieved by adding of 10 μM GOx in water to a solution composed of maghemite nanoparticles with a mass concentration of 200 mg l^{-1} and bound to 99.75 μmol of RITC per 1 g of FeNp; the as-prepared solution was then left under stirring overnight at 4 °C. The unbound enzyme was removed by extensive nanoparticle washing in the presence of an external magnetic field. After three washing cycles, the activity of the immobilized enzyme was found to be constant. The result was supported by the activity measurements. The amount of leached GOx was assessed by controlling the residual activity of the enzyme in the washing buffer solution, and was found to be less than 1%.

The activity of the enzyme after immobilization was calculated by measuring the rate of the GOx catalyzing oxidation of β-D-glucose. In particular, the initial reaction rate was measured as a function of the substrate concentration determining the hydrogen peroxide production in the presence of free and/or immobilized enzyme. The measurements of the immobilized enzyme activity were performed under continuous stirring. The reaction rate was independent of the stirring rate, thus implying that the kinetics of the reaction is not diffusion-controlled. Under the above-mentioned experimental conditions, the immobilized enzyme showed a catalytic rate constant of 32.7 s^{-1} toward glucose oxidation. As a key practical aspect, FeNp-RITC-GOx complexes were simply removed from the solution by an application of an external magnet and activity measurements were repeated by monitoring the disappearance of fluorescence from the assay solution. After various cycles, the bound enzyme maintains its activity, thus demonstrating the reusability of the GOx immobilized on the magnetic fluorescent complexes (see Fig. 7).

Microscopic observations of the FeNp-RITC-GOx nanocomposite (see Fig. 8) illustrate a change in the character of the organic shell after GOx binding. The higher fraction of organic phase on a particle surface is clearly reflected in the increased shell thickness (5–9 nm) and also in the lower contrast of nanoparticles themselves, which are more embedded in the organic matrix. The shell thickness is in good agreement with the calculated size of GOx ($7 \times 5.5 \times 8$ nm^3) [65].

The aggregated character of the coated nanoparticles, as shown in Fig. 8, is due to the TEM sample pre-treatment and drying on the carbon-coated grid because the nanoparticles still maintain their

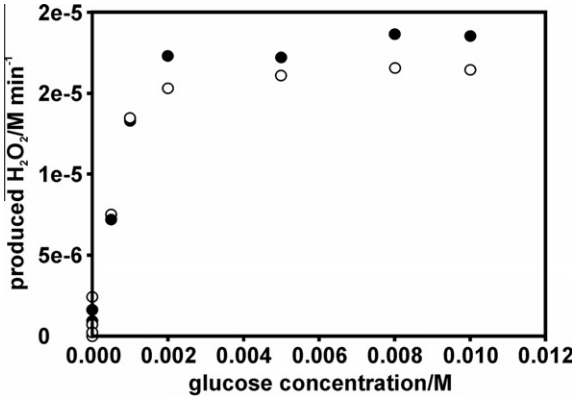

Fig. 7. Comparison of the catalytic (enzymatic) activity of the FeNp-RITC-GOx complex, where ● corresponds to freshly prepared nanoparticles and ○ corresponds to nanoparticles separated after the catalytic action by an external magnet and re-used.

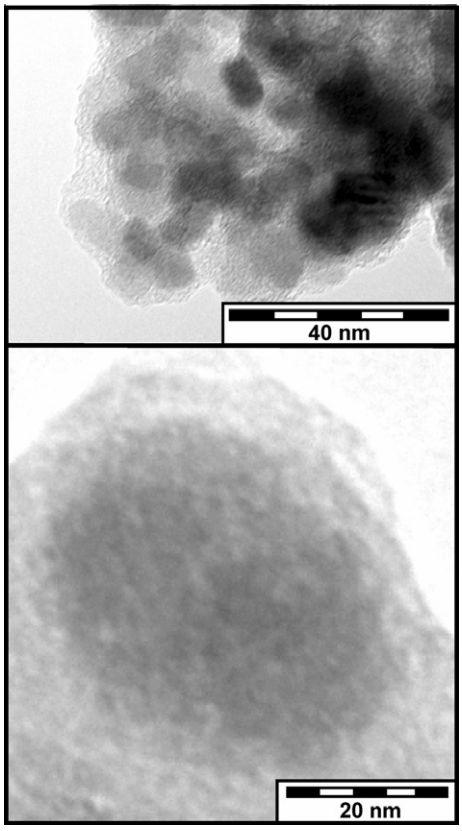

Fig. 8. TEM images of the FeNp-RITC-GOx nanoparticles demonstrating the glucose oxidase shell on the rhodamine-modified maghemite nanoparticles.

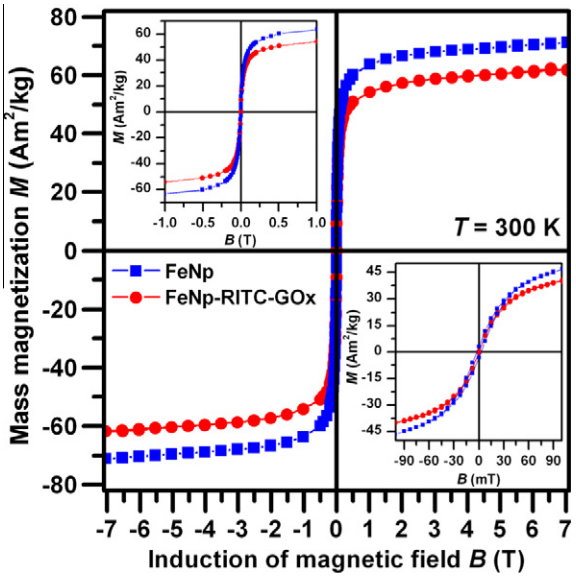

Fig. 9. Comparison of the room-temperature hysteresis loops recorded for the native maghemite particles and for the FeNp-RITC-GOx fluorescent magnetic carrier.

great colloidal characteristics. The fluorescence properties of the native RITC are well reflected in the behaviour of the FeNp-RITC-GOx nanocomposite showing the comparable fluorescence characteristics (see Supporting information, Fig. S4). Moreover, the magnetic properties of the FeNp-RITC-GOx complex are also very favorable for targeted controlling as proved by the field

dependence of magnetization measured at 300 K (see Fig. 9). Compared to the native maghemite nanoparticles, the maximum magnetization decreased from ~71.4 $Am^2 kg^{-1}$ to ~60.2 $Am^2 kg^{-1}$ for the FeNp-RITC-GOx system. With respect to a diamagnetic nature of organic phases (RITC and GOx), these magnetic data allow us to quantify the content of organic phases bound to the maghemite surface. The found value of ~15 wt.% is in good correspondence with TG data (not shown). The amount of GOx immobilized on the maghemite-rhodamine nanoparticles was independently determined by exploiting the specific characteristics of the enzyme [56]. The enzyme is characterized by the presence of two FAD molecules, bound to the protein structure via non-covalent bonds that can be weakened in an acidic environment. Based on the fluorescence determination of the released enzyme cofactor (FAD), we found 10.6 ± 2.0 nmol ($n = 3$) of GOx on 14.6 mg of the FeNp-RITC-GOx system, corresponding to 10 ± 2 molecules per nanoparticle. These results suggest the formation of a monomolecular layer of GOx bound to stoichiometric maghemite nanoparticles. An average amount of 11.7 wt.% of GOx was calculated. Considering that the amount of bound rhodamine was 2.5 wt.% of the whole FeNp-RITC-GOx complex, these data are in excellent agreement with magnetization measurements discussed above.

4. Conclusions

- We report a unique synthetic route towards maghemite nanoparticles stabilized by OH^- groups and exhibiting excellent colloidal behaviour without any additional organic or inorganic modification of their surface. The developed approach does not require any organic solvents, high cost polymers (surfactants) and/or expensive instrumentation.
- The negative charge of the surface OH^- groups can be exploited for a simple electrostatic immobilization of the positively charged organic molecules. In this way, RITC as a fluorescent label was attached, resulting in a fluorescent magnetically drivable nanocarrier. This is the first reported example of magnetic fluorescent nanoparticles based on the rhodamine structure allowing the covalent attachment of various biomolecules.
- Exploiting the chemical properties of the isothiocyanate functionality, glucose oxidase was covalently bound to RITC to develop the first magnetically controllable rhodamine-based nanocatalyst (see Fig. 10).
- The immobilized enzyme, as a monomolecular layer, retains its catalytic activity towards oxidation of β-D-glucose. The prepared fluorescent magnetically drivable nanocatalyst might be easily used to remove molecular oxygen from aqueous solutions in the case of glucose excess. The presence of the nanocatalyst can be conveniently monitored by its fluorescence. Moreover, the nanocatalyst can be quickly removed by the application of a simple external magnet and re-used several times without a loss of the catalytic efficiency. The developed magnetic fluorescent biosensor can be exploited in many food chemistry applications, such as low ethanol wine production or gluconic acid production [66,67].

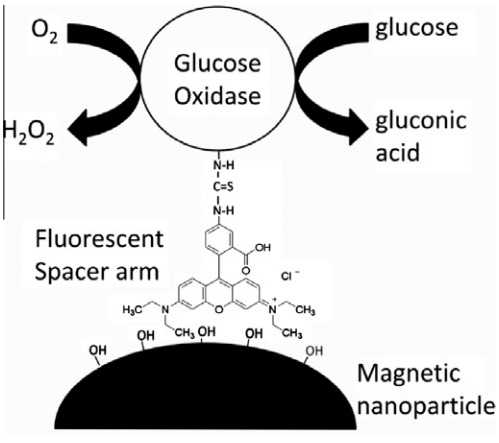

Fig. 10. Simplified scheme of the fluorescent magnetically drivable nanocatalyst.

Acknowledgements

This work was funded in part by Progetti di Ateneo by the University of Padua. The authors gratefully acknowledge the support by the Operational Program Research and Development for Innovations – European Development Fund (Project No. CZ.1.05/2.1.00/03.0058) of the Ministry of Education, Youth, and Sports of the Czech Republic. This work has been also supported by the Ministry of Education, Youth, and Sports of the Czech Republic (Project Nos. 1M6198959201 and MSM6198959218) and the Academy of Sciences of the Czech Republic (Project No. KAN115600801).

Appendix A. Figures with essential colour discrimination

Certain figures in this article, particularly Figs. [2–5 and 9], are difficult to interpret in black and white. The full colour images can be found in the online version, at doi:10.1016/j.actbio.2012. 02.005.

Appendix B. Supplementary data

Supplementary data associated with this article can be found, in the online version, at doi:10.1016/j.actbio.2012.02.005.

References

[1] Gupta AK, Gupta M. Synthesis and surface engineering of iron oxide nanoparticles for biomedical applications. Biomaterials 2005;26:3995–4021.
[2] Pankhurst QA, Connolly J, Jones SK, Dobson J. Applications of magnetic nanoparticles in biomedicine. J Phys D Appl Phys 2003;36:R167–81.
[3] Lu AH, Salabas EL, Schuth F. Magnetic nanoparticles: synthesis, protection, functionalization, and application. Angew Chem Int Ed 2007;46:1222–44.
[4] Laurent S, Forge D, Port M, Roch A, Robic C, Elst LV, et al. Magnetic iron oxide nanoparticles: synthesis, stabilization, vectorization, physicochemical characterization and biochemical applications. Chem Rev 2008;108:2064–110.
[5] Mornet S, Vasseur S, Grasset F, Duguet E. Magnetic nanoparticle design for medical diagnosis and therapy. J Mater Chem 2004;14:2161–75.
[6] Thorek DLJ, Chen A, Czupryna J, Tsourkas A. Superparamagnetic iron oxide nanoparticle probes for molecular imaging. Ann Biomed Eng 2006;34:23–38.
[7] Cai WB, Chen XY. Nanoplatforms for targeted molecular imaging in living subjects. Small 2007;3:1840–54.
[8] Riehemann K, Schneider SW, Luger TA, Godin B, Ferrari M, Fuchs H. Nanomedicine-challenge and perspectives. Angew Chem Int Ed 2009;48:872–97.
[9] Wunderbaldinger P, Josephson L, Weissleder R. Crosslinked iron oxides (CLIO): a new platform for the development of targeted MR contrast agents. Acad Radiol 2002;9:S304–6.
[10] Schellenberger EA, Bogdanov AJ, Hogemann D, Tait J, Weissleder R, Josephson L, et al. Annexin V–CLIO: a nanoparticle for detecting apoptosis by MRI. Mol Imaging 2002;2:102–7.
[11] Kooi ME, Cappendijk VC, Cleutjens KB, Kessels AG, Kitslaar PJ, Borgers M, et al. Accumulation of ultrasmall superparamagnetic particles of iron oxide in human atherosclerotic plaques can be detected by *in vivo* magnetic resonance imaging. Circulation 2003;107:2453–8.
[12] Keller TM, Michel SC, Frohlich J, Fink D, Caduff R, Marincek B, et al. USPIO-Enhanced MRI for preoperative staging of gynecological pelvic tumors: preliminary results. Eur Radiol 2004;14:937–44.
[13] Larsen EKU, Nielsen T, Wittenborn T, Birkedal H, Vorup-Jensen T, Jakobsen MH, et al. Size-dependent accumulation of PEGylated silane-coated magnetic iron oxide nanoparticles in murine tumors. ACS Nano 2009;3:1947–51.
[14] Funovics MA, Kapeller B, Hoeller C, Su HS, Kunstfeld R, Puig S, et al. MR imaging of the Her2/neu and 9.2.27 tumor antigens using immunospecific contrast agents. Magn Reson Imaging 2004;22:843–50.
[15] Krause MH, Kwong KK, Gragoudas ES, Young LH. MRI of blood volume with superparamagnetic iron in choroidal melanoma treated with thermotherapy. Magn Reson Imaging 2004;22:779–87.

[16] Lunov O, Syrovets T, Büchele B, Jiang X, Röcker C, Tron K, et al. The effect of carboxydextran-coated superparamagnetic iron oxide nanoparticles on c-Jun N-terminal kinase-mediated apoptosis in human macrophages. Biomaterials 2010;31:5063–71.
[17] Lewin M, Carlesso N, Tung CH, Tang XW, Cory D, Scadden DT, et al. Tat peptide-derivatized magnetic nanoparticles allow *in vivo* tracking and recovery of progenitor cells. Nat Biotechnol 2000;18:410–4.
[18] Lu CW, Hung Y, Hsiao JK, Yao M, Chung TH, Lin YS, et al. Bifunctional magnetic silica nanoparticles for highly efficient human stem cell labeling. Nano Lett 2007;7:149–54.
[19] Sun LP, Zborowski M, Moore LR, Chalmers JJ. Continuous, flow-through immunomagnetic cell sorting in a quadrupole field. Cytometry 1998;33: 469–75.
[20] McCloskey KE, Chalmers JJ, Zborowski M. Magnetic cell separation: characterization of magnetophoretic mobility. Anal Chem 2003;75:6868–74.
[21] Jordan A, Scholz R, Wust P, Fahling H, Felix R. Magnetic fluid hyperthermia (MFH): cancer treatment with AC magnetic field induced excitation of biocompatible superparamagnetic nanoparticles. J Magn Magn Mater 1999;201:413–9.
[22] Kim J, Grate JW, Wang P. Nanostructures for enzyme stabilization. Chem Eng Sci 2006;61:1017–26.
[23] Bornscheuer UT. Immobilizing enzymes: how to create more suitable biocatalysts. Angew Chem Int Ed 2003;42:3336–7.
[24] Liu XQ, Ma ZY, Xing JM, Liu HZ. Preparation and characterization of amino-silane modified superparamagnetic silica nanospheres. J Magn Magn Mater 2004;270:1–6.
[25] Rossi LM, Quach AD, Rosenzweig Z. Glucose oxidase-magnetite nanoparticle bioconjugate for glucose sensing. Anal Bioanal Chem 2004;380:606–13.
[26] Safarik I, Safarikova M. Magnetic nanoparticles and biosciences. Mon Chem 2002;133:737–59.
[27] Kluchova K, Zboril R, Tucek J, Pecova M, Zajoncova L, Safarik I, et al. Superparamagnetic maghemite nanoparticles from solid-state synthesis – Their functionalization towards peroral MRI contrast agent and magnetic carrier for trypsin immobilization. Biomaterials 2009;30:2855–63.
[28] Li D, Teoh WY, Gooding JJ, Selomulya C, Amal R. Functionalization strategies for protease immobilization on magnetic nanoparticles. Adv Funct Mater 2010;20:1767–77.
[29] Zhao LY, Zhang YJ, Wei JY, Cao D, Liu KH, Qian XH. Rapid isolation and identification method for blocked N-terminal peptides by isothiocyanate-coupled magnetic nanoparticles and MS. Proteomics 2009;9:4416–20.
[30] Mani V, Chikkaveeraiah BV, Patel V, Gutkind JS, Rusling JF. Ultrasensitive immunosensor for cancer biomarker proteins using gold nanoparticle film electrodes and multienzyme-particle amplification. ACS Nano 2009;3: 585–94.
[31] Kouassi G, Irudayaraj J, McCarty G. Activity of glucose oxidase functionalized onto magnetic nanoparticles. Biomagn Res Technol 2005;3:1–10.
[32] Tsang SC, Yu CH, Gao X, Tam K. Silica-encapsulated nanomagnetic particles as a new recoverable biocatalyst carrier. J Phys Chem B 2006;110:16914–22.
[33] Katz E, Willner I. Integrated nanoparticle-biomolecule hybrid systems: Synthesis, properties, and applications. Angew Chem Int Ed 2004;43: 6042–108.
[34] Astalan AP, Ahrentorp F, Johansson C, Larsson K, Krozer A. Biomolecular reactions studied using changes in Brownian rotation dynamics of magnetic particles. Biosens Bioelectron 2004;19:945–51.
[35] Hrbac J, Halouzka V, Zboril R, Papadopoulos K, Triantis T. Carbon electrodes modified by nanoscopic iron(III) oxides to assemble chemical sensors for the hydrogen peroxide amperometric detection. Electroanalysis 2007;19:1850–4.
[36] Wang J. Electrochemical glucose biosensors. Chem Rev 2008;108:814–25.
[37] Baby TT, Ramaprabhu S. SiO_2 coated Fe_3O_4 magnetic nanoparticle dispersed multiwalled carbon nanotubes based amperometric glucose biosensor. Talanta 2010;80:2016–22.
[38] Liu Z, Wang J, Xie D, Chen G. Polyaniline-coated Fe_3O_4 nanoparticle-carbon-nanotube composite and its application in electrochemical biosensing. Small 2008;4:462–6.
[39] Barone PW, Strano MS. Single walled carbon nanotubes as reporters for the optical detection of glucose. J Diabetes Sci Technol 2009;3:242–52.
[40] Jennings LE, Long NJ. "Two is better than one" – Probes for dual-modality molecular imaging. Chem Commun 2009;p. 3511–24.
[41] Liong M, Lu J, Kovochich M, Xia T, Ruehm SG, Nel AE, et al. Multifunctional inorganic nanoparticles for imaging, targeting, and drug delivery. ACS Nano 2008;2:889–96.
[42] Erogbogbo F, Yong KT, Hu R, Law WC, Ding H, Chang CW, et al. Biocompatible magnetofluorescent probes: luminescent silicon quantum dots coupled with superparamagnetic iron(III) oxide. ACS Nano 2010;4:5131–8.
[43] Insin N, Tracy JB, Lee H, Zimmer JP, Westervelt RM, Bawendi MG. Incorporation of iron oxide nanoplarticles and quantum dots into silica microspheres. ACS Nano 2008;2:197–202.
[44] Landmark KJ, DiMaggio S, Ward J, Kelly CV, Vogt S, Hong S, et al. Synthesis, characterization, and in vitro testing of superparamagnetic iron oxide nanoparticles targeted using folic acid-conjugated dendrimers. ACS Nano 2008;2:773–83.
[45] Sun CR, Du K, Fang C, Bhattarai N, Veiseh O, Kievit F, et al. PEG-mediated synthesis of highly dispersive multifunctional superparamagnetic nanoparticles: their physicochemical properties and function *in vivo*. ACS Nano 2010;4:2402–10.
[46] Cho HS, Dong ZY, Pauletti GM, Zhang JM, Xu H, Gu HC, et al. Fluorescent, superparamagnetic nanospheres for drug storage, targeting, and imaging: a multifunctional nanocarrier system for cancer diagnosis and treatment. ACS Nano 2010;4:5398–404.
[47] Krichevsky O, Bonnet G. Fluorescence correlation spectroscopy: the technique and its applications. Rep Prog Phys 2002;5:251–97.
[48] Ke JH, Lin JJ, Carey JR, Chen JS, Chen CY, Wang LF. A specific tumor-targeting magnetofluorescent nanoprobe for dual-modality molecular imaging. Biomaterials 2010;31:1707–15.
[49] Gupta MN, Kaloti M, Kapoor M, Solanki K. Nanomaterials as matrices for enzyme immobilization. Artif Cells Blood Substit Biotechnol 2011;39:98–109.
[50] Ansari SA, Husain Q. Potential applications of enzymes immobilized on/in nano materials: a review. Biotechnol Adv 2011. doi:10.1016/j.biotechadv.2011.09.005.
[51] Cash KJ, Clark HA. Nanosensors and nanomaterials for monitoring glucose in diabetes. Trends Mol Med 2010;16:584–93.
[52] Li JP, Wei XP, Yuan YH. Synthesis of magnetic nanoparticles composed by Prussian Blue and glucose oxidase for preparing highly sensitive and selective glucose biosensor. Sens Actuator B Chem 2009;139:400–6.
[53] Fang M, Grant PS, McShane MJ, Sukhorukov GB, Golub VO, Lvov YM. Magnetic bio/nanoreactor with multilayer shells of glucose oxidase and inorganic nanoparticles. Langmuir 2002;18:6338–44.
[54] Swovada BER, Massey VJ. Purification and properties of glucose oxidase from *Aspergillus niger*. J Biol Chem 1965;240:2209–15.
[55] Sober HA, Harte RA. CRC handbook of biochemistry. 2nd edn. Cleveland, OH: The Chemical Rubber Co.; 1970.
[56] Vianello F, Bortoluzzi S, Zennaro L, Rigo A. Determination of glucose oxidase immobilized as monolayer onto a flat surface. J Biochem Biophys Methods 2002;51:263–71.
[57] Morris DL, Buckler RT. Colorimetric immunoassay using a flavin adenine dinucleotide as label. Methods Enzymol 1983;92:413–25.
[58] Stevanato R, Mondovi' B, Sabatini S, Rigo A. Spectrophotometric assay for total polyamines by immobilized amine oxidases. Anal Chim Acta 1990;237:391–7.
[59] Zboril R, Mashlan M, Petridis D. Iron(III) oxides from thermal processes: synthesis, structural and magnetic properties, Mössbauer spectroscopy characterization, and applications. Chem Mater 2002;14:969–82.
[60] Tucek J, Zboril R, Petridis D. Maghemite nanoparticles by view of Mössbauer spectroscopy. J Nanosci Nanotechnol 2006;6:926–47.
[61] Mornet S, Portier J, Duguet E. A method for synthesis and functionalization of ultrasmall superparamagnetic covalent carriers based on maghemite and dextran. J Magn Magn Mater 2005;293:127–34.
[62] Roca AG, Marco JF, Morales MP, Serna CJ. Effect of nature and particle size on properties of uniform magnetite and maghemite nanoparticles. J Phys Chem 2007;111:18577–84.
[63] Daou TJ, Greneche JM, Pourroy G, Buathong S, Derory A, Ulhaq-Bouillet C, et al. Coupling agent effect on magnetic properties of functionalized magnetite-based nanoparticles. Chem Mater 2008;20:5869–75.
[64] Raba J, Mottola HA. Glucose oxidase as an analytical reagent. Crit Rev Anal Chem 1995;25:1–42.
[65] Hecht HR, Kalisz HM, Hendle J, Schmid RD, Schomburg D. Crystal structure of glucose oxidase from *Aspergillus Niger* refined at 2.3 Å. J Mol Biol 1993;229:153–72.
[66] Wong CM, Wong KH, Chen XD. Glucose oxidase: natural occurrence, function, properties and industrial applications. Appl Microbiol Biotechnol 2008;78: 927–38.
[67] Sandip BB, Mahesh VB, Rekha SS, Laxmi A. Glucose oxidase – An overview. Biotechnol Adv 2009;27:489–501.